Journal of Rare Earths xxx (xxxx) xxx

Contents lists available at ScienceDirect

Journal of Rare Earths

journal homepage: http://www.journals.elsevier.com/journal-of-rare-earths

Catalytic combustion of toluene on Pt/Al_2O_3 and Pd/Al_2O_3 catalysts with CeO_2, CeO_2–Y_2O_3 and La_2O_3 as coatings☆

Bing Zhou [a, b], Quanli Ke [a], Meijun Wen [a], Tianbiao Ying [a], Guokai Cui [a], Ying Zhou [a], Zhenyu Gu [b], Hanfeng Lu [a, *]

[a] Institute of Catalytic Reaction Engineering, College of Chemical Engineering, Zhejiang University of Technology, Hangzhou 310014, China
[b] Key Laboratory of Environmental Pollution Control Technology Research of Zhejiang Province, Eco-environmental Science Research & Design Institute of Zhejiang Province, Hangzhou 310007, China

ARTICLE INFO

Article history:
Received 14 March 2022
Received in revised form
10 May 2022
Accepted 14 May 2022
Available online xxx

Keywords:
Volatile organic compounds
Catalytic oxidization
Carrier modification
$Pt/Ce–Al_2O_3$
Rare earths

ABSTRACT

CeO_2, La_2O_3, and CeO_2–Y_2O_3 oxides were coated on the surface of spherical granular Al_2O_3 (3–5 mm) through impregnation method, and proved as better supports of Pd and Pt catalysts. The influences of rare earth metal doping on the adsorption rates of Pd and Pt ions, as well as the catalytic performance, were investigated. Results show that the $H_2PtCl_6·6H_2O$ adsorption rates of the Al_2O_3 carriers modified by Ce, La, and CeY increase significantly. These rare earth coatings can adsorb almost all $H_2PtCl_6·6H_2O$ in the solution. Compared with Pt/Al_2O_3 catalyst, $Pt/Ce–Al_2O_3$ and $Pt/CeY–Al_2O_3$ catalysts have better degradation performance for toluene, and the T_{90} temperatures are both about 147 °C. According to X-ray photoelectron spectroscopy (XPS) characterization, Pt^0 is an important active species for catalytic oxidation reaction of toluene. After CeO_2 modification to the conventional Pt/Al_2O_3 catalyst, the proportion of Pt^0 increases from 74.5% to 82.1%. When the Pt^0 content in the metal state is improved, the redox activity of the catalyst is promoted correspondingly.

1. Introduction

Volatile organic compounds (VOCs) have great damage to human health and the environment. They may cause impairments of the blood, skin, gastrointestinal tract, cardiovascular system and central nervous system when entering the human body through inhalation, ingestion and skin absorption.[1–4] At present, low concentration is a typical characteristic of waste gas from industrial emissions containing VOCs. Conventional methods to deal with such industrial waste gases include adsorption, photocatalysis, and plasma method.[5–7] However, all of these methods have certain disadvantages, such as the low degradation rate, high infrastructure investment and severe safety concerns.[8–10] In recent years, catalytic oxidation has attracted increasing attention as an environmentally friendly and highly efficient technology to deal with waste gas. Nevertheless, catalytic oxidation generally requires a relatively high temperature, thereby resulting in high energy consumption and safety issues.[11–15] Therefore, VOCs degradation under low-temperature or even room-temperature catalytic oxidation is becoming the objective of scientific researchers.[16–20]

The core of low-temperature catalytic oxidation is the development of catalysts. Currently, supported catalysts are frequently applied in practice.[21–24] Among them, Pd and Pt have excellent catalytic performances as active components in eliminating VOCs such as toluene.[25–28] Besides, activated alumina balls (3–5 mm) are the most common support in industries because they have high specific surface area, low price, and good compatibility of active components and, in addition, ability of improving the dispersity of precious metals.[24] Modifying activated alumina balls by selecting appropriate promoters to further lower the catalytic oxidation temperature of conventional Pd/Al_2O_3 and Pt/Al_2O_3 catalysts is a hotspot of research nowadays.[29,30] Relevant studies have been conducted continuously. For example, the synergistic effect between the Pd and Co phases in the $Pd–Co/\gamma\text{-}Al_2O_3$ catalyst was investigated and the binary-metal catalyst shows excellent catalytic oxidation activity toward toluene.[31] Moreover, the doping of CeO_2

☆ **Foundation item:** Project supported by the Scientific Research Fund of Zhejiang Provincial Education Department (Y202043197), the National Natural Science Foundation of China (22078294), the Natural Science Foundation of Zhejiang Province (LZ21E080001, LGF20E080018) and the Key Laboratory of Environmental Pollution Control Technology Research of Zhejiang Province (2021ZEKL04).

* Corresponding author.
E-mail address: luhf@zjut.edu.cn (H. Lu).

https://doi.org/10.1016/j.jre.2022.05.007
1002-0721/

is beneficial to the dispersion of Pd particles on Al_2O_3 support. For instance, a relatively high oxygen storage capacity brings higher catalytic activity to the propane oxidation steam reforming of Pd/CeO_2–Al_2O_3.[32] Abbasi et al.[33] prepared a Pt/Al_2O_3–CeO_2 nanocatalyst through impregnation method, which was used in catalytic combustion of BTX with varied CeO_2 contents. The researchers found that CeO_2 and Pt not only had a synergistic effect but also promoted the redox activity of the supported catalyst. Temperature of only 250 °C was needed for complete transformation of toluene when Ce content was 30%, and high removal rate could be realized under different BTX concentrations. Next to CeO_2, CeO_2–Y_2O_3 and La_2O_3 can also significantly strengthen metal-support interaction, and change the dispersity, chemical valence and mechanical strength of active species. However, few studies have focused on the formation of bimetallic or polymetallic components of CeO_2, CeO_2–Y_2O_3, and La_2O_3 with Pd and Pt on Al_2O_3 support and systematically investigated the consequent impact on the reaction activity.

In this study, influences of Ce, CeY and La modification on the catalytic activity of conventional Pd/Al_2O_3 and Pt/Al_2O_3 catalysts as well as adsorption rates of aqueous Pd and Pt ions were investigated. Moreover, characterization analyses of catalysts were conducted by using X-ray diffraction (XRD), scanning electron microscopy (SEM), transmission electron microscopy (TEM), and X-ray photoelectron spectroscopy (XPS). Influences of Pt loading on the catalytic activity of toluene were investigated and the thermostability of the catalyst was further studied.

2. Experimental

2.1. Preparation of catalysts

The blank active alumina balls were rinsed with deionized water and then processed by an ultrasonic cleaner for 30 min. Then, they were cleaned and dried for later use.

2.1.1. Pd/Al_2O_3 catalyst

0.2 wt% Pd/Al_2O_3 was prepared. Specifically, 5 g Al_2O_3 was taken, to which 20 mL of 0.5 g/L chloropalladium acid solution was added. Pd ions were adsorbed in 75 °C water bath (shaking and stirring the solution continuously to ensure that Pd ion concentration was uniform). After a certain period, Pd ion concentration was tested by UV–vis until Pd ions were adsorbed basically. The catalysts were roasted for 4 h at 400 and 800 °C.

2.1.2. Pd/La–Al_2O_3 catalyst

In this section, 0.2 mol/L $La(NO_3)_3$ aqueous solution was prepared and 10 g Al_2O_3 was immersed in the $La(NO_3)_3$ aqueous solution for 5 h. The aqueous solution only had to immerse solids completely. Next, the solution was filtered. Samples were dried at 100 °C and then roasted at 400 °C for 4 h, thus getting La–Al_2O_3 carrier. The preparation methods of Pd/La–Al_2O_3 catalysts were the same as the Pd/Al_2O_3 catalyst.

2.1.3. Pd/Ce–Al_2O_3 catalyst

In this section, 1.0 mol/L $Ce(NO_3)_2$ aqueous solution was prepared and 10 g Al_2O_3 was immersed in the $Ce(NO_3)_2$ aqueous solution for 5 h. The aqueous solution only had to immerse solids completely. Then, the solution was filtered. Samples were dried at 100 °C and then roasted at 400 °C for 4 h, thereby obtaining Ce–Al_2O_3 carrier. The preparation methods of Pd/Ce–Al_2O_3 catalysts were the same as the Pd/Al_2O_3 catalyst.

2.1.4. Pd/CeY–Al_2O_3 catalyst

In this section, 1.0 mol/L $Ce(NO_3)_2$ and $Y(NO_3)_2$ aqueous solutions were prepared (Ce accounted for 0.75 mol/L and Y accounted for 0.25 mol/L) and 10 g Al_2O_3 was immersed in the Ce–Y aqueous solution for 5 h. The aqueous solution only had to immerse solids completely. Then, the solution was filtered. Samples were dried at 100 °C and then roasted at 400 °C for 4 h, thereby obtaining a CeY–Al_2O_3 carrier. The preparation methods of Pd/CeY–Al_2O_3 catalysts were the same as that of the Pd/Al_2O_3 catalyst.

The preparation methods of Pt catalysts were the same as the preceding method.

2.2. Characterization of catalysts

The XRD characterization was implemented on an X'Pert PRO X-ray diffractometer (PANalytical Company, Netherlands). The spherical particle catalysts were broken to form powder samples. Ni filtering was tested and Kα ray (λ = 0.1541 nm), which was generated by Cu target, was used to trigger samples to develop diffraction. The tube voltage, current, scanning range, and scanning speed were set at 40 kV, 40 mA, 10°–80°, and 0.02 (°)/s, respectively.

Sample morphology was characterized by SEM (S-4700 (II), Hitachi, Japan). The field emission voltage was 29.0 kV. Samples should be cut and processed by metal spraying before the test.

TEM characterization of samples was performed on a Tecnai G2 F30 S-Twin high-resolution transmission electron microscope, and the test voltage was 120 kV.

H_2-temperature programmed reduction (H_2-TPR) was tested on an Autochem 3010E (Zhejiang Fine-Tech Instruments, China). A desired amount of sample (100 mg) was placed in a quartz reactor, pretreated in a flow of Ar gas at 200 °C for 2 h, and cooled to 50 °C. A gas mixture of H_2 (5%) and Ar (95%) then passed (30 mL/min) through the reactor. The temperature was increased from 50 to 900 °C at a heating rate of 10 °C/min. A TCD detector was used at the outlet of the reactor to measure the volume of hydrogen consumed during reduction.

The metal binding energy of samples and surface metal concentration were analyzed by a VG Scientific ESCALab220i-XL electron spectroscope for chemical analysis. The spherical particle catalysts were broken to form powder samples. The excitation source used the Al Kα X-ray and power was approximately 300 W. The basic vacuum at analysis was 3×10^{-7} Pa. The C 1s (284.6 eV) was used as internal standard to correct the electronic binding energy.

The texture properties of catalysts include specific surface area, pore volume, pore diameter, and total porosity, which were analyzed on a 3Flex surface property analyzer (Micromeritics). Total porosity was measured by an −196 °C N_2 absorption/desorption isotherm. Before the experiment, samples were degasified in vacuum at 150 °C for 8 h. Specific surface area of samples was obtained by the BET model.

Quantitative analysis by a Shimadzu spectrophotometer was used to measure loading capacities of Pt and Pd and external standard method was applied. First, different concentrations of Pt and Pd solutions (g/L) were used as standard samples. According to their absorbance at WL = 316 nm, the absorbance marking lines of Pt and Pd were gained to test contents of Pt and Pd in residual solution.

2.3. Catalytic activity measurement

The activity test of catalysts in toluene combustion was performed on the fixed bed reactor. The air steel cylinder extended two paths of air. One path was connected to a bubble bottle with

toluene through the mass flowmeter and bubbles under 0 °C generate toluene steam, which was mixed and diluted with air in another path to obtain the desired inlet concentration of toluene. The diluted toluene concentration was 2000 ppm and the total air flow rate was 191 mL/min. Then, the diluted toluene was further supplied into a U-shaped reaction tube with catalyst. Specifically, the inner diameter of the U-shaped reaction tube was 18 mm, the catalyst dosage was approximately 2.0 g, and the airspeed was 3000 h^{-1}. The inlet and outlet concentrations of toluene were tested by an Agilent 6890 gas chromatograph equipped with an FID detector.

3. Results and discussion

3.1. Adsorption of Pt and Pb ions

The adsorption tests of Pt and Pd ions on different supports (Al_2O_3 support and Al_2O_3 supports modified by Ce, La, and CeY) were discussed through their adsorption capacities of $H_2PtCl_6·6H_2O$ and H_2PdCl_4 (Fig. 1). Fig. 1(a) shows that the Al_2O_3 carrier has poor adsorption to $H_2PtCl_6·6H_2O$ and it could only adsorb all $H_2PtCl_6·6H_2O$ onto the carrier surface after approximately 1800 min. Some studies demonstrate that the $H_2PtCl_6·6H_2O$ adsorption rate of the Al_2O_3 carrier is related to the isoelectric point. The isoelectric points (pH_{PZC}) and pH values of several substances are listed in Table 1. As the isoelectric point of the Al_2O_3 carrier is approximately 6, the Al_2O_3 surface has positive charges when pH of the solution is lower than 6, which is beneficial to $PtCl_6^{2-}$ producing electrostatic adsorption on the OH^-—$Al_{(s)}$ surface. $H_2PtCl_6·6H_2O$ is adsorbed according to the following formula[34]:

$$2OH^-—Al_{(s)} + H_2PtCl_{6(l)} \rightarrow Al—PtCl_6^{2-}—Al_{(s)} + 2H_2O \quad (1)$$

On the contrary, Al_2O_3 has negative charges when pH is higher than 6, which strengthens repulsion to anions, thereby decreasing the electrostatic adsorption capacity. $H_2PtCl_6·6H_2O$ is adsorbed according to the following formula:

$$2OH^-_{(s)} + PtCl_6^{2-}{}_{(l)} \rightarrow Pt(OH)_{4(s)}\downarrow + 4Cl^-_{(l)} \quad (2)$$

The pH value of the impregnation liquid for the unmodified Al_2O_3 carrier increases gradually with the increase of $H_2PtCl_6·6H_2O$ adsorption time. When the pH value approaches the isoelectric point of the Al_2O_3 carrier, the adsorption rate of Pt decreases gradually. However, the $H_2PtCl_6·6H_2O$ adsorption rates of the Al_2O_3 carriers modified by Ce, La, and CeY increase significantly. At 100 min, it can adsorb almost all $H_2PtCl_6·6H_2O$ in the solution. The enhanced adsorption capacity of the support for the $H_2PtCl_6·6H_2O$, after modifications by Ce, La and CeY, can be attributed to changes of isoelectric points on the Al_2O_3 carrier surface. In the adsorption process, the initial pH value of $H_2PtCl_6·6H_2O$ is 2.47. When the carrier reaches saturation of $H_2PtCl_6·6H_2O$ adsorption, the ultimate pH value of the solution is approximately 5.8. As the isoelectric points of CeO_2, La_2O_3, and Y_2O_3 are higher than 5.8, the Al_2O_3 carriers modified by Ce, La, and CeY have good adsorption capacities of $H_2PtCl_6·6H_2O$. On the other hand, Fig. 1(b) shows that the H_2PdCl_4 adsorption capacity of the unmodified Al_2O_3 carrier differs slightly from those of the Al_2O_3 carrier modified by Ce, La, and CeY. At 60 min, almost all carriers can adsorb Pd ions in the solution completely because the pH value of the H_2PdCl_4 solution has relatively strong acidity. H^+ in the solution can easily interact with OH^- on the Al_2O_3 surface, thereby making the $PdCl_4^{2-}$ precipitate on the carrier surface.

Table 1
The isoelectric point or pH of several substances.

Samples	pH_{PZC}	pH
Active alumina balls	6.0	/
La_2O_3	10	/
CeO_2	6.7–8.6	/
Y_2O_3	7.15–8.95	/
$H_2PtCl_6·6H_2O$	/	2.47
H_2PdCl_4	/	1.4
Deionized water	/	7

3.2. Evaluation for activity

The evaluation results of Pd- and Pt-based catalysts on the catalytic combustion performance of toluene are shown in Fig. 2 and Table 2. Catalytic activity results were analyzed by T_{10}, T_{50}, and T_{90} (the transformation rates of toluene were 10%, 50%, and 90% of the reaction temperatures). Results demonstrated that the toluene catalytic activity of conventional Pd/Al_2O_3 catalysts decreased after doping of Ce, La, and CeY. Especially, an obvious activity reduction was witnessed in Pd/Al_2O_3 catalyst modified by La and its T_{90} increased by 32 °C. Moreover, toluene catalytic activity of conventional Pd/Al_2O_3 catalysts modified by La also decreases to a certain extent. On the contrary, when Pt was used as the active species alternatively, modification by Ce and CeY is more beneficial to the catalytic combustion of toluene of the Pt/Al_2O_3 catalyst. This study mainly investigated the catalytic degradation performances of toluene on the catalysts with Ce and CeY coating modifications.

Based on the preceding analysis, the Ce- and CeY-modified carriers present similar catalytic degradation performances

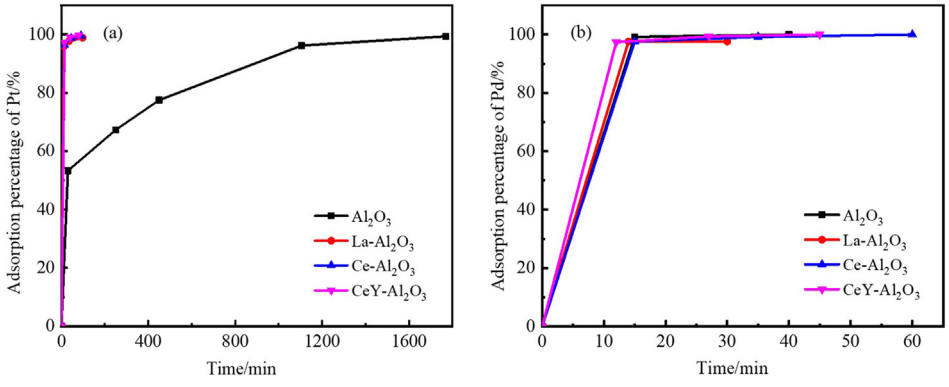

Fig. 1. Pt and Pd ions adsorption performances on Al_2O_3 and Al_2O_3 modified by rare earth oxides. (a) $H_2PtCl_6·6H_2O$; (b) H_2PdCl_4.

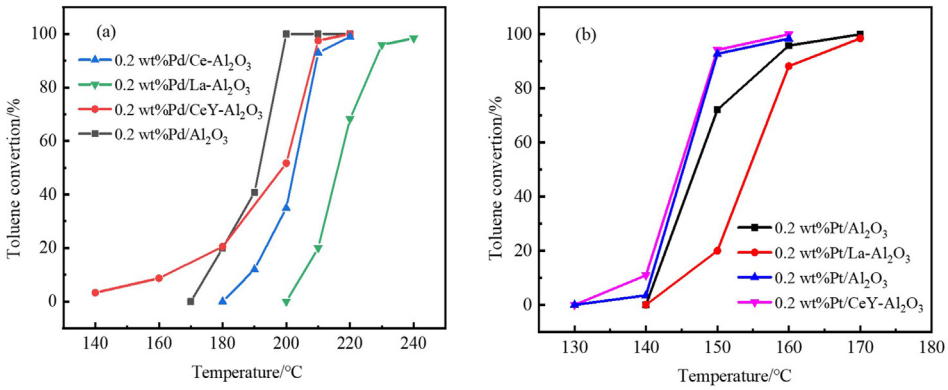

Fig. 2. Catalytic combustion of toluene over Pd and Pt catalysts after calcination at 400 °C.

Table 2
T_{10}, T_{50} and T_{90} of Pd and Pt catalysts calcined at 400 °C.

Samples	T_{10} (°C)	T_{50} (°C)	T_{90} (°C)
0.2 wt%Pd/Al_2O_3	175	189	196
0.2 wt%Pd/La–Al_2O_3	210	217	228
0.2 wt%Pd/Ce–Al_2O_3	190	201	206
0.2 wt%Pd/CeY–Al_2O_3	160	198	205
0.2 wt%Pt/Al_2O_3	142	147	153
0.2 wt%Pt/La–Al_2O_3	143	155	159
0.2 wt%Pt/Ce–Al_2O_3	141	143	147
0.2 wt%Pt/CeY–Al_2O_3	140	143	147
0.1 wt%Pt/CeY–Al_2O_3	150	166	178
0.3 wt%Pt/CeY–Al_2O_3	136	143	147
0.4 wt%Pt/CeY–Al_2O_3	140	143	147
0.5 wt%Pt/CeY–Al_2O_3	130	136	147
0.01 wt%Pt/Ce–Al_2O_3	160	205	230
0.05 wt%Pt/Ce–Al_2O_3	146	167	178
0.1 wt%Pt/Ce–Al_2O_3	141	143	147

toward toluene. Therefore, the 0.2 wt% Pt/CeY–Al_2O_3 catalyst was first selected and the influence of Pt loadings on catalytic degradation activity of toluene was examined. Results are shown in Fig. 3 and Table 2. Clearly, the catalyst activity of catalyst with 0.1 wt% Pt loading is the lowest. Its T_{10}, T_{50}, and T_{90} increased by 10, 21, and 28 °C compared with those catalysts with 0.2 wt% Pt loading. The reason might be that the active component content is extremely low and the active sites are inadequate, and they cannot well activate oxygen and VOCs. Based on the catalytic results on sample with 0.2 wt% Pt loading, increasing the Pt loadings continuously failed to improve the catalytic performance toward toluene because excessive Pt loadings may decrease the Pt dispersion on the carrier surface.

According to the above analysis, excessive Pt loadings cannot promote catalytic degradation activity of toluene to a certain extent. Meanwhile, investigating the influences of Pt loadings on the degradation activity of toluene is important, as this reflects the industrilization potential of catalyst. Meanwhile, the catalytic activity of Pt/CeY–Al_2O_3 catalyst decreases obviously when the mass fraction of Pt is 0.1 wt%. Therefore, a low-loading experiment was conducted by selecting the Pt/Ce–Al_2O_3 catalyst, which proves to have good catalytic performance. Results are shown in Fig. 3 and Table 2. Clearly, in presence of low Pt loadings, the activity of the Pt/Ce–Al_2O_3 catalyst increases with the Pt loading increasing. The catalytic activities of toluene are the same when the mass fraction of Pt is 0.1 wt% and 0.2 wt%, indicating that further increasing Pt loadings over 0.1 wt% cannot improve the catalytic performance of toluene. To sum up, the activities of the Pt/CeY–Al_2O_3 and Pt/Ce–Al_2O_3 catalysts are not positively related to Pt loadings. Through this experiment, the optimal Pt loading was chosen, which can reduce cost and is significant for practical industrial application of catalysts.

3.3. Thermal stability test

Evaluation of toluene catalytic combustion performances of Pd- and Pt-based catalysts after calcination under 800 °C is shown in Fig. 4 and Table 3. After high-temperature calcination, the catalytic oxidation activity of the conventional Pd/Al_2O_3 catalyst to toluene is improved. Combined with XPS data in Fig. 10(a), the proportion of Pd^{2+} is speculated to increase after high-temperature calcination

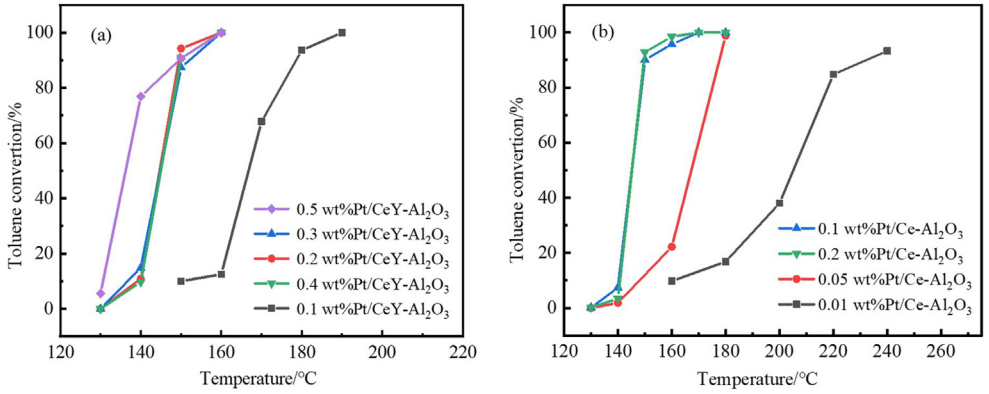

Fig. 3. Catalytic combustion of toluene over Pt/CeY–Al_2O_3 and Pt/Ce–Al_2O_3 after calcination at 400 °C.

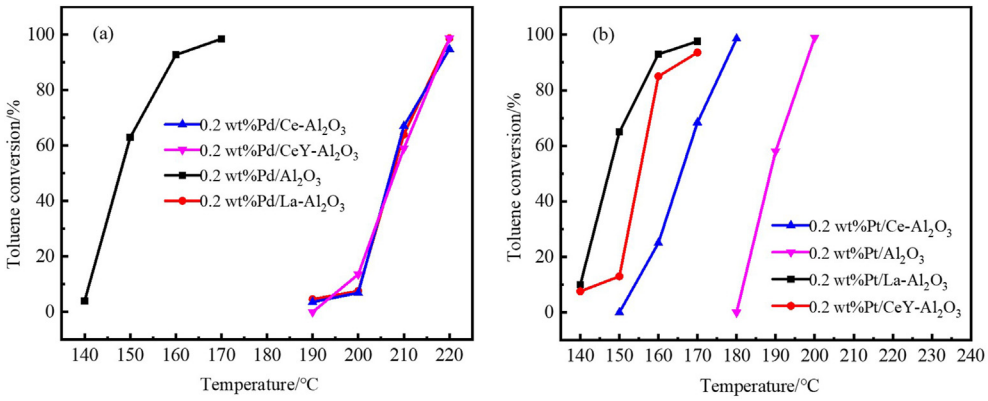

Fig. 4. Catalytic combustion of toluene over Pd and Pt catalysts after calcination at 800 °C.

Table 3
T_{10}, T_{50} and T_{90} of Pd and Pt catalysts calcined at 800 °C.

Samples	T_{10} (°C)	T_{50} (°C)	T_{90} (°C)
0.2 wt%Pd/Al_2O_3	141	147	156
0.2 wt%Pd/La–Al_2O_3	200	208	217
0.2 wt%Pd/Ce–Al_2O_3	200	208	217
0.2 wt%Pd/CeY–Al_2O_3	197	208	217
0.2 wt%Pt/Al_2O_3	181	188	197
0.2 wt%Pt/La–Al_2O_3	140	147	155
0.2 wt%Pt/Ce–Al_2O_3	154	165	175
0.2 wt%Pt/CeY–Al_2O_3	140	155	163

and the increased PdO content is the key factor. Meanwhile, T_{90} of the Pd catalysts modified by Ce and CeY only increased by 11 and 12 °C after high-temperature calcination, which indicates that Ce and CeY modifications are beneficial to maintaining high-temperature catalysis activity of conventional Pd/Al_2O_3 catalysts for toluene degradation. Compared with conventional Pd/Al_2O_3 catalysts, the catalytic activity of the conventional Pt/Al_2O_3 catalyst to toluene after high-temperature calcination declines significantly. By combining the XPS data of Fig. 10(b), one can speculate that the proportion of Pt^{2+} increases after high-temperature calcination and the decreased Pt^0 content in metal state is the major reason. T_{90} values of Pt catalysts after Ce and CeY modifications and high-temperature calcination only increase by 28 and 16 °C. This result reveals that Ce and CeY modifications are also beneficial to maintaining the high-temperature catalytic activity of conventional Pt/Al_2O_3 catalysts. An important result is that T_{90} of conventional Pd/Al_2O_3 and Pt/Al_2O_3 catalysts modified by La after high-temperature calcination slightly decreases, which indicates that La modification is significant in maintaining the high-temperature catalytic activity of conventional Pd and Pt catalysts.

3.4. Catalyst characterization

When Pt was used as the active species alternatively, modification by Ce is more beneficial to the catalytic combustion of toluene of the Pt/Al_2O_3 catalyst. The photos of monolithic catalysts of Pt/Al_2O_3 and Pt/Ce–Al_2O_3 are shown in Fig. 5. Al_2O_3 and Pt/Ce–Al_2O_3 were chosen for XRD characterization. The XRD spectra are shown in Fig. 6. Clearly, the pristine Al_2O_3 develops diffraction peaks near $2\theta = 13.933°$, 28.332°, 38.477°, and 49.214°, indicating that pristine Al_2O_3 is pseudo-boehmite (α-AlOOH). The calcined Pt/Ce–Al_2O_3 catalyst has diffraction peaks near $2\theta = 37.59°$, 39.47°, 45.84°, and 67.00°, showing the γ-Al_2O_3 characteristic peaks. In addition, the Pt/Ce–Al_2O_3 catalyst has diffraction peaks of CeO_2

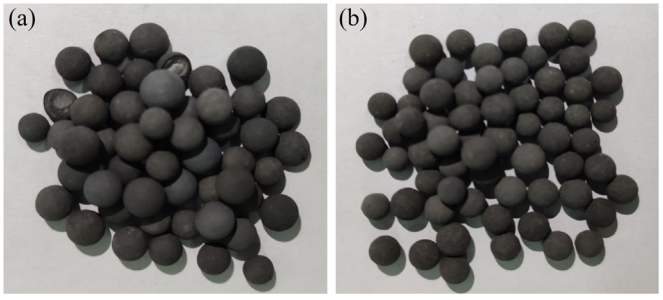

Fig. 5. The photos of monolithic catalysts. (a) Pt/Al_2O_3; (b) Pt/Ce–Al_2O_3.

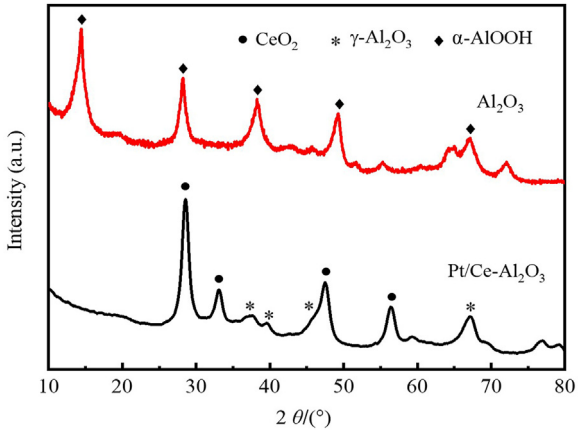

Fig. 6. XRD patterns of Al_2O_3 and Pt/Ce–Al_2O_3.

near $2\theta = 28.8°$, 33.4°, 47.6°, and 56.6°. However, the characteristic diffraction peak of Pt was not detected probably due to the low Pt contents in samples.

To study surface morphological changes of carriers before and after modification, this study conducted SEM characterization of Al_2O_3 and Pt/Ce–Al_2O_3 samples (Fig. 7). Fig. 7(a) and (b) show that the unloaded activated aluminum oxide has relatively rough surface and pore channels in different sizes. These pore channels can effectively adsorb active components in the impregnation liquid. The surface morphology of the Pt/Ce–Al_2O_3 catalyst is shown in Fig. 7(c) and (d). The study found that CeO_2 exists on the Al_2O_3 carrier surface as a layer of thin film and the loads are uniform. Due to the small content of the Ce coating, γ-Al_2O_3 and CeO_2 were chosen as probe supports in this study for further characterization

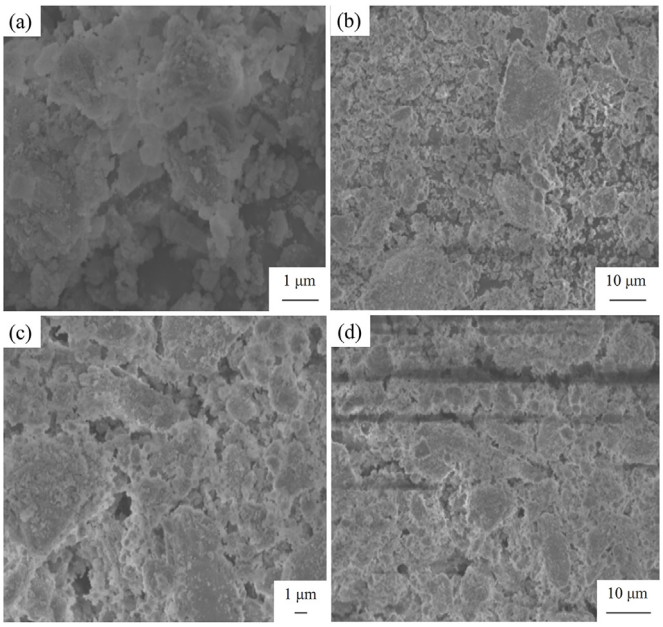

Fig. 7. SEM images of Al_2O_3 and Pt/Ce–Al_2O_3. (a, b) Al_2O_3; (c, d) Pt/Ce–Al_2O_3.

to investigate the interaction between precious metal particles and real supports.

The distributions of Pd and Pt grain sizes can be observed from TEM images. Pd/γ-Al_2O_3, Pd/CeO_2, Pt/γ-Al_2O_3, and Pt/CeO_2 were selected for TEM characteristic analysis (Fig. 8). Fig. 8(a) and (b) show that Pd particles are found on the γ-Al_2O_3 and CeO_2, with grain size ranging between 10 and 18 nm. Fig. 8(c) and (d) show that there are Pt particles on γ-Al_2O_3 and CeO_2, with grain size ranging between 8 and 15 nm. The grain sizes of Pd and Pt on the two supports are slightly different, indicating that the supports have minor influences on the Pd and Pt grains. This result proves that the grain sizes of Pd and Pt are not major influencing factors in the activity of catalysts.

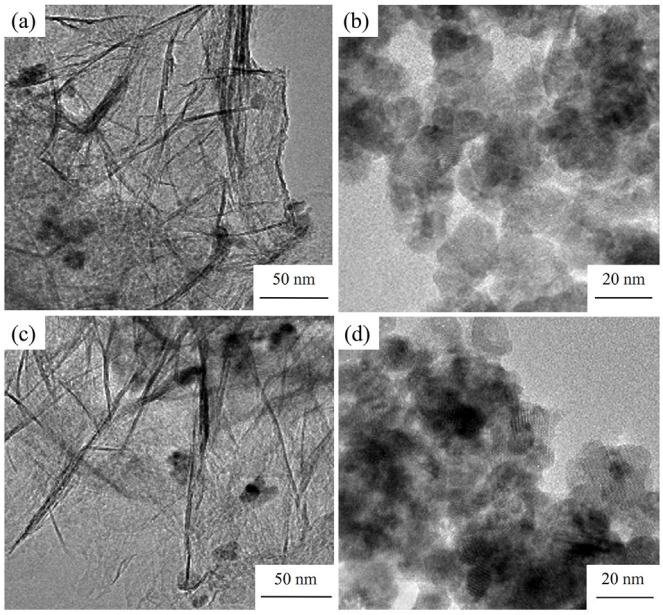

Fig. 8. TEM images of Pd/γ-Al_2O_3, Pd/CeO_2, Pt/γ-Al_2O_3 and Pt/CeO_2. (a) Pd/γ-Al_2O_3; (b) Pd/CeO_2; (c) Pt/γ-Al_2O_3; (d) Pt/CeO_2.

The H_2-TPR profiles of the different catalysts were investigated and are shown in Fig. 9. The Pt/Al_2O_3 catalyst shows one peak centered at about 446 °C, which can be assigned to the reduction of Pt. For the Pt/CeO_2 catalyst, three peaks appear centered at about 88, 384, and 771 °C. The peak at 384 °C can be assigned to the reduction of surface CeO_2. The high temperature peak at 771 °C can be attributed to the reduction of bulk CeO_2 to Ce_2O_3.[35,36] In comparison to the Pt/Al_2O_3 catalyst, the redox capacity of Pt/CeO_2 is significantly improved.

XPS spectra of Pd on Pd/γ-Al_2O_3 and Pd/CeO_2 are shown in Fig. 10(a) and Table 4. The Pd $3d_{5/2}$ and Pd $3d_{3/2}$ peaks of the electronic binding energy at 335.4 and 340.7 eV can be attributed to Pd^0 in metal state. The Pd $3d_{5/2}$ and Pd $3d_{3/2}$ peaks of the electronic binding energy at 336.2 eV and 341.5 eV might be attributed to Pd^{2+} in the oxidation state.[37] The XPS spectra of Pt on Pt/γ-Al_2O_3 and Pt/CeO_2 are shown in Fig. 10(b) and Table 4. As the electronic binding energy of Al 2p distributes in the similar range with that of Pt 4f, the Pt 4f peak overlaps in a broad Al 2p background peak, making it impossible to separate their peaks accurately. Thus, Pt 4d was used as reference for XPS analysis. The Pt $4d_{5/2}$ and Pt $4d_{3/2}$ peaks of the electronic binding energy at 314.3 and 330.9 eV might be attributed to Pt^0 in the metal state, while the Pt $4d_{5/2}$ and Pt $4d_{3/2}$ peaks of the electronic binding energy at 317.5 and 333.9 eV might be attributed to Pt^{2+} in the oxidation state. Table 4 shows that after CeO_2 modification of conventional Pd/Al_2O_3 catalyst, the proportion of Pd^{2+} decreases from 57.16% to 51.23% and the PdO content decreases. At present, there is no consensus on the effects of metal state and oxidation state of Pd on oxidation reaction.[38–40] In this study, the XPS results, together with the activity data in Fig. 2(a), indicate that Pd^{2+} is at least an important species for catalytic oxidation reaction of toluene. The catalytic activity of toluene declines as the PdO content decreases after modification by Ce, La, and CeY.[41–43] Table 4 shows that after CeO_2 modification to the conventional Pt/Al_2O_3 catalyst, the proportion of Pt^0 increases from 74.5% to 82.1% and the Pt^0 content in the metal state increases. Existing studies on the catalytic oxidation reaction of Pt fails to obtain a consistent conclusion on whether the active species is Pt^0 or Pt^{2+}. Combined with active data in Fig. 2(b), Pt^0 is the important active species for catalytic oxidation reaction of toluene. As the Pt^0 content decreases after La modification, the catalytic activity of toluene declines correspondingly. The Pt^0 content increases after modification by Ce and CeY, which is more beneficial to the catalytic combustion of toluene.

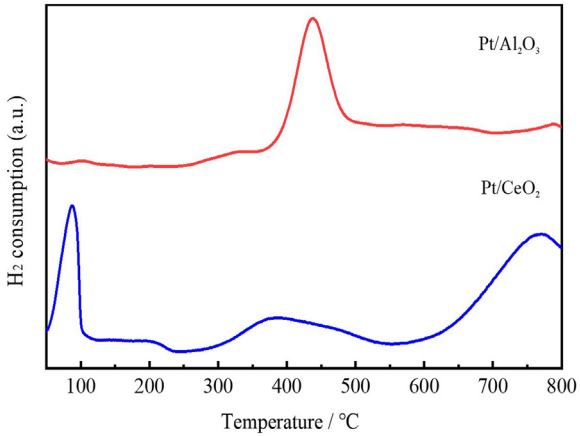

Fig. 9. H_2-TPR profiles of Pt/Al_2O_3 and Pt/CeO_2 catalysts.

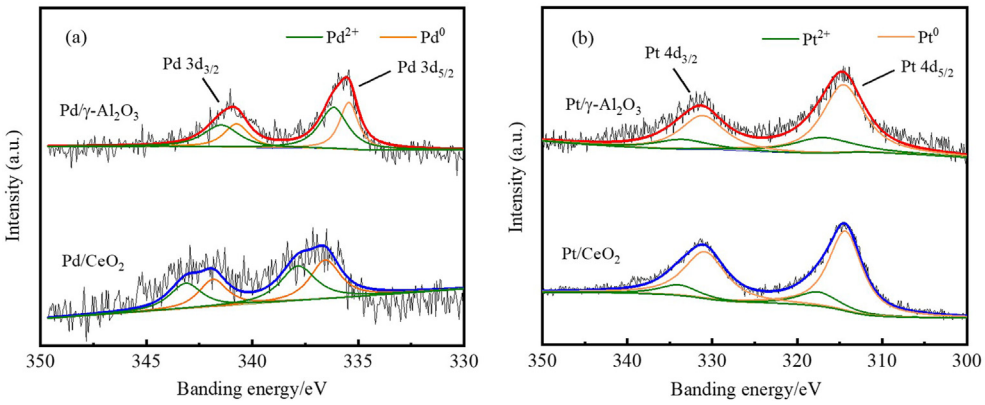

Fig. 10. XPS spectra of Pd 3d for Pd/γ-Al_2O_3 and Pd/CeO_2 (a) and Pt 4d for Pt/γ-Al_2O_3 and Pt/CeO_2 (b).

Table 4
XPS analysis of Pd/γ-Al_2O_3, Pd/CeO_2, Pt/γ-Al_2O_3 and Pt/CeO_2.

Samples	Content of surface species	
	$Pd^{2+}/(Pd^0+Pd^{2+})$ (%)	$Pt^0/(Pt^0+Pt^{2+})$ (%)
Pd/γ-Al_2O_3	57.16	/
Pd/CeO_2	51.23	/
Pt/γ-Al_2O_3	/	74.5
Pt/CeO_2	/	82.1

4. Conclusions

Active alumina balls were selected as the catalyst support and rare earth elements including Ce, La, and CeY were doped for modification. After modification, the Pt ion adsorption rate on the activated alumina balls increases significantly. However, it has little influences on the adsorption rate of the Pd ions. This result is mainly related to isoelectric points. For the Pt/Al_2O_3 catalyst, however, Ce and CeY modifications are more beneficial to catalytic combustion for toluene, which is mainly related to the varied proportion of Pt^0/Pt^{2+}. Specifically, the Pt/Ce−Al_2O_3 catalyst shows the most excellent catalytic oxidation performance for toluene. Its T_{90} temperature is around 147 °C, which is 6 °C lower than that of the conventional Pt/Al_2O_3 catalyst.

References

1. Guo MM, Li K, Zhang HB, Min X, Liang JX, Hu XF, et al. Promotional removal of oxygenated VOC over manganese-based multi oxides from spent lithium-ions manganate batteries: modification with Fe, Bi and Ce dopants. *Sci Total Environ*. 2020;740, 139951.
2. Zhang CY, Chu W, Chen F, Li L, Jiang RY, Yan JL. Effects of cerium precursors on surface properties of mesoporous $CeMnO_x$ catalysts for toluene combustion. *J Rare Earths*. 2020;38:70.
3. Lin FW, Zhang ZM, Li N, Yan BB, He C, Hao ZP, et al. How to achieve complete elimination of Cl-VOCs: a critical review on byproducts formation and inhibition strategies during catalytic oxidation. *Chem Eng J*. 2021;404, 126534.
4. Dong F, Han WG, Guo Y, Han WL, Tang ZC. $CeCoO_x$-MNS catalyst derived from three-dimensional mesh nanosheet Co-based metal−organic frameworks for highly efficient catalytic combustion of VOCs. *Chem Eng J*. 2021;405, 126948.
5. Muir B, Sobczyk M, Bajda T. Fundamental features of mesoporous functional materials influencing the efficiency of removal of VOCs from aqueous systems: a review. *Sci Total Environ*. 2021;784, 147121.
6. Liu BY, Ji J, Zhang BG, Huang WJ, Gan YL, Leung DYC, et al. Catalytic ozonation of VOCs at low temperature: a comprehensive review. *J Hazard Mater*. 2022;422, 126847.
7. Cheng TY, Li JJ, Ma XW, Zhou L, Wu H, Yang LJ. Alkylation modified pistachio shell-based biochar to promote the adsorption of VOCs in high humidity environment. *Environ Pollut*. 2022;295, 118714.
8. Cheng SF, Lu F, Peng P, Zheng J. Emission characteristics and control scenario analysis of VOCs from heavy-duty diesel trucks. *J Environ Manag*. 2021;293, 112915.
9. Wang Y, Yang DY, Li SZ, Chen MQ, Guo LM, Zhou J. Ru/hierarchical HZSM-5 zeolite as efficient bi-functional adsorbent/catalyst for bulky aromatic VOCs elimination. *Microporous Mesoporous Mater*. 2018;258:17.
10. Brown RW, Bull LD, Journeaux T, Chadwick DR, Jones DL. Volatile organic compounds (VOCs) allow sensitive differentiation of biological soil quality. *Soil Boil Biochem*. 2021;156, 108187.
11. Feng SY, Liu JD, Gao B. Synergistic mechanism of Cu-Mn-Ce oxides in mesoporous ceramic base catalyst for VOCs microwave catalytic combustion. *Chem Eng J*. 2022;429, 132302.
12. Chen L, Liao YF, Xin SR, Song XX, Liu GC, Ma XQ. Simultaneous removal of NO and volatile organic compounds (VOCs) by Ce/Mo doping-modified selective catalytic reduction (SCR) catalysts in denitrification zone of coal-fired flue gas. *Fuel*. 2020;262, 116485.
13. Chen L, Liao YF, Chen Y, Wu JN, Ma XQ. Performance of Ce-modified V-W-Ti type catalyst on simultaneous control of NO and typical VOCS. *Fuel Process Techonl*. 2020;207, 106483.
14. Shayegan Z, Haghighat F, Li CS. Surface fluorinated Ce-doped TiO_2 nanostructure photocatalyst: a trap and remove strategy to enhance the VOC removal from indoor air environment. *Chem Eng J*. 2020;401, 125932.
15. Li SD, Wang DD, Wu XF, Chen YF. Recent advance on VOCs oxidation over layered double hydroxides derived mixed metal oxides. *Chin J Catal*. 2020;41:550.
16. Gaálová J, Topka P, Kaluža L, Soukup K, Barbier J. Effect of gold loading on ceria-zirconia support in total oxidation of VOCs. *Catal Today*. 2019;333:190.
17. Yang CT, Miao G, Pi YH, Xia QB, Wu JL, Li Z, et al. Abatement of various types of VOCs by adsorption/catalytic oxidation: a review. *Chem Eng J*. 2019;370:1128.
18. Wang QY, Yeung KL, Bañares MA. Ceria and its related materials for VOC catalytic combustion: a review. *Catal Today*. 2020;356:141.
19. Cuo ZX, Deng YZ, Li WH, Peng SP, Zhao F, Liu HD, et al. Monolithic Mn/Ce-based catalyst of fibrous ceramic membrane for complete oxidation of benzene. *Appl Surf Sci*. 2018;456:594.
20. Gelin MF, Blokhin AP, Ostrozhenkova E, Apolonski A, Maiti KS. Spectrochimica acta Part A: molecular and biomolecular spectroscopy. *Spectrochim Acta*. 2021;258, 119785.
21. Ren S, Liang WJ, Fang HF, Zhu YX. Performance and poisoning analysis of organic sulfur resistance of Pd-Ce catalyst in catalytic oxidation of VOCs. *J Environ Chem Eng*. 2021;9, 106640.
22. Xi K, Wang Y, Jiang K, Xie J, Zhou Y, Lu HF. Support interaction of Pt/CeO_2 and Pt/SiC catalysts prepared by nano platinum colloid deposition for CO oxidation. *J Rare Earths*. 2020;38:376.
23. Yang Y, Wang G, Fang D, Han JN, Dang F, Yang M. Study of the use of a Pd−Pt-based catalyst for the catalytic combustion of storage tank VOCs. *Int J Hydrogen Energy*. 2020;45:22732.
24. Zhu AM, Zhou Y, Wang Y, Zhu QL, Liu HY, Zhang ZK, et al. Catalytic combustion of VOCs on Pt/CuMnCe and Pt/CeY honeycomb monolithic catalysts. *J Rare Earths*. 2018;36:1272.
25. Shi YJ, Wang JL, Zhou RX. Pt-support interaction and nanoparticle size effect in Pt/CeO_2−TiO_2 catalysts for low temperature VOCs removal. *Chemosphere*. 2021;265, 129127.
26. Zhang SS, Pu WH, Chen A, Xu Y, Wang YY, Yang CZ, et al. Oxygen vacancies enhanced photocatalytic activity towards VOCs oxidation over Pt deposited Bi_2WO_6 under visible light. *J Hazard Mater*. 2020;384, 121478.
27. Liu GZ, Tian YJ, Zhang BF, Wang L, Zhang XW. Catalytic combustion of VOC on sandwich-structured Pt@ZSM-5 nanosheets prepared by controllable intercalation. *J Hazard Mater*. 2019;367:568.
28. Chen X, Li JY, Wang Y, Zhou Y, Zhu QL, Lu HF. Preparation of nickel-foam-supported Pd/NiO monolithic catalyst and construction of novel electric heating reactor for catalytic combustion of VOCs. *Appl Catal A-Gen*. 2020;607, 117839.

29. Gan T, Chu XF, Qi H, Zhang WX, Zou YC, Yan WF, et al. Pt/Al_2O_3 with ultralow Pt-loading catalyze toluene oxidation: promotional synergistic effect of Pt nanoparticles and Al_2O_3 support. *Appl Catal, B*. 2019;257, 117943.
30. Weng XY, Shi BQ, Liu AN. Highly dispersed Pd/modified-Al_2O_3 catalyst on complete oxidation of toluene: role of basic sites and mechanism insight. *Appl Surf Sci*. 2019;497, 143747.
31. Stefanov P, Todorova S, Naydenov A. On the development of active and stable Pd-Co/γ-Al_2O_3 catalyst for complete oxidation of methane. *Chem Eng J*. 2015;266:329.
32. Faria WLS, Perez CAC, César DV. *In situ* characterizations of Pd/Al_2O_3 and $Pd/CeO_2/Al_2O_3$ catalysts for oxidative steam reforming of propane. *Appl Catal, B*. 2009;92:217.
33. Abbasi Z, Haghighi M, Fatehifar E, Saedy S. Synthesis and physicochemical characterizations of nanostructured Pt/Al_2O_3–CeO_2 catalysts for total oxidation of VOCs. *J Hazard Mater*. 2011;186:1445.
34. Bozon-Verduraz F, Omar A, Escard J. Chemical state and reactivity of supported palladium: I. Characterization by XPS and uv-visible spectroscopy. *J Catal*. 1978;53:126.
35. Luo MF, He M, Xie YL, Fang P, Jin LY. Toluene oxidation on Pd catalysts supported by CeO_2-Y_2O_3, washcoated cordierite honeycomb. *Appl Catal B Environ*. 2007;69:213.
36. Lu HF, Kong XX, Huang HF, Zhou Y, Chen YF. Cu-Mn-Ce ternary mixed-oxide catalysts for catalytic combustion of toluene. *J Environ Sci*. 2015;32:102.
37. Pacanowski S, Wachowiak M, Jablonski B. Interface mixing and hydrogen absorption in Pd/Mg and Pd/Al/Mg thin films. *Int J Hydrogen Energy*. 2021;46:806.
38. Kinnunen NM, Suvanto M, Moreno MA. Methane oxidation on alumina supported palladium catalysts: effect of Pd precursor and solvent. *Appl Catal A-Gen*. 2009;370:78.
39. Okumura K, Kobayashi T, Tanaka H. Toluene combustion over palladium supported on various metal oxide supports. *Appl Catal, B*. 2003;44:325.
40. Zhang M, Cai SC, Li JJ, Elimian EA, Chen J, Jia HP. Ternary multifunctional catalysts of polymeric carbon nitride coupled with Pt-embedded transition metal oxide to enhance light-driven photothermal catalytic degradation of VOCs. *J Hazard Mater*. 2021;412, 125266.
41. Yazawa Y, Yoshida H, Takagi N. Acid strength of support materials as a factor controlling oxidation state of palladium catalyst for propane combustion. *J Catal*. 1999;187:15.
42. Jamnani SR, Moghaddam HM, Leonardi SG, Neri G. A novel conductometric sensor based on hierarchical self-assembly nanoparticles Sm_2O_3 for VOCs monitoring. *Ceram Int*. 2018;44:16953.
43. Jiang RX, Xie ZK, Zhang CF. Characterization and performance of Pd-La/spinel catalyst for preparation of 2,6-diisopropylaniline. *Appl Catal A-Gen*. 2003;250:209.